Supporting Information

Cefiderocol under siege? Understanding the rise of NDM-mediated resistance

Brenda A. Warecki[1], Pablo E. Tomatis[1,2], María F. Mojica[3,4,5], Christopher R. Bethel[5], Magdalena Rodríguez Saravia[6], Salvador Drusin[2,7], Daisuke Ono[5,8], Guillermo Bahr[1], Krisztina Papp-Wallace[5, 8,9], Pranita D. Tamma[10], Diego M. Moreno[2,7], Graciela Mahler[6], Robert A. Bonomo[3,4,5,8,9,10,11] and Alejandro J. Vila[1,2,4]*

[1] Instituto de Biología Molecular y Celular de Rosario (IBR), CONICET, Universidad Nacional de Rosario, Rosario, Argentina

[2] Facultad de Ciencias Bioquímicas y Farmacéuticas, Universidad Nacional de Rosario, Rosario, Argentina

[3] Department of Molecular Biology and Microbiology, Case Western Reserve University School of Medicine, Cleveland, Ohio, USA

[4] CWRU-Cleveland VAMC Center for Antimicrobial Resistance and Epidemiology (Case VA CARES), Cleveland, Ohio, USA

[5] Research Service, Veterans Affairs Northeast Ohio Healthcare System, Cleveland, Ohio, USA

[6] Facultad de Química, Universidad de la República, Montevideo, Uruguay.

[7] Instituto de Química Rosario (IQUIR), CONICET, Universidad Nacional de Rosario, Rosario, Argentina.

[8] Department of Medicine, Case Western Reserve University School of Medicine, Cleveland, Ohio, USA

[9] Department Biochemistry, Case Western Reserve University School of Medicine, Cleveland, Ohio, USA

[10] Department of Pediatrics, Division of Infectious Diseases, Johns Hopkins University School of Medicine, Baltimore, Maryland, USA

[11] Departments of Pharmacology, Proteomics and Bioinformatics, Case Western Reserve University School of Medicine, Cleveland, Ohio, USA

[12] Clinician Scientist Investigator, Veterans Affairs Northeast Ohio Healthcare System, Cleveland, Ohio, USA

*To whom correspondence should be addressed: Alejandro J. Vila (vila@ibr-conicet.gov.ar) and Robert A. Bonomo (rab14@case.edu).

Class	Enzyme	K_m (μM)	k_{cat} (s^{-1})	k_{cat}/K_m (M^{-1} s^{-1})	*Ref*
A	KPC-2	> 500	> 0.03	5 x10^1	[1]
	KPC-33	3	0.006	2 x10^3	[1]
	KPC-3	> 500	> 0.13	2.5 x10^2	[1]
	KPC-31	12	0.008	6.6 x10^2	[1]
	PER-1			7.6x10^4	[2]
	PER-2			7.2x10^4	[2]
	CMY-185			3x10^4	[3]
B	**VIM-2**	**248**	**1.1**	**4.4x10^3**	**This work**
	IMP-1	**302**	**1.25**	**4.1x10^3**	**This work**
	NDM-1	**429**	**84.2**	**1.96x10^5**	**This work**
	NDM-5	**405**	**78.2**	**1.93x10^5**	**This work**
	NDM-1	161	11	0.7x10^5	[4]
	NDM-9	53	7	1.3x10^5	[4]
	VIM-1	295	1.17	4.0x10^3	[5]
	VIM-24			5.0x10^3	[6]
	L1	510	12	2.4x10^4	[7]
	AmpC	533	0.08	1.5x10^2	[8]
C	$AmpC^{Ent385}$	49.8	0.14	2.8x10^3	[8]
D	OXA-23	4,800	--	--	[7]

Table S1. Comparison of catalytic parameters of FDC hydrolysis by different β-lactamases.

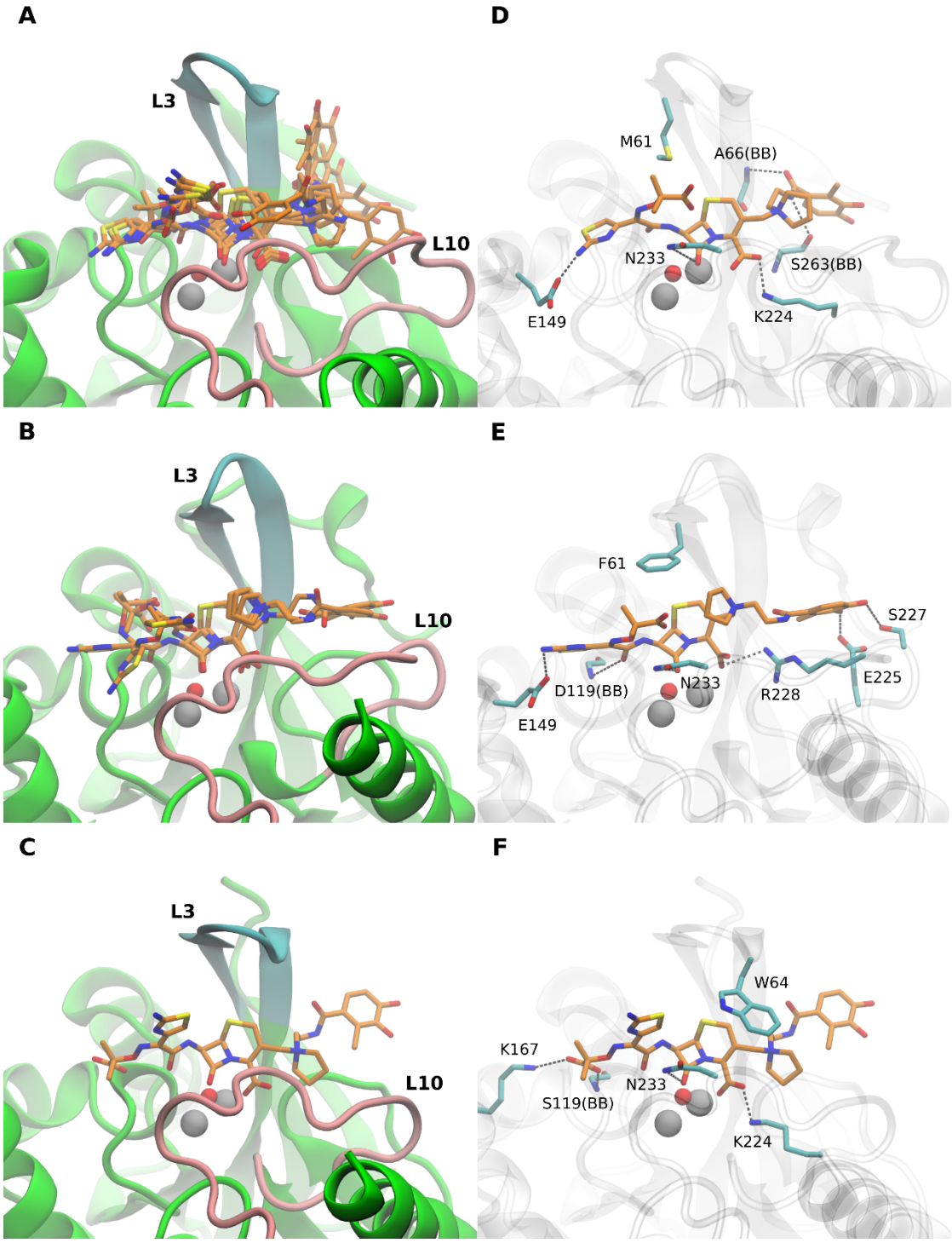

Figure S1. Docking simulations of FDC in the active sites of (A) NDM-1, (B) VIM-2 and (C) IMP-1. Carbon atoms of FDC are colored in orange, loop L3 in the protein in cyan, loop L10 loop in magenta, and the rest of the protein in green. Several productive docking poses were obtained for NDM-1 and VIM-2. All poses were superimposed in the cavity of the active site showing that FDC can explore many conformations. In IMP-1 only one productive pose was obtained indicating a more restrictive active site. The lowest energy poses are shown for clarity. **FDC-protein interactions in (D) NDM-1, (E) VIM-2 and (F) IMP-1.** Carbon atoms of FDC are colored in orange while those of each protein are colored in cyan. Hydrogen bonds are shown as

dotted lines and interactions with residue backbones are denoted with (BB). To better illustrate the interactions, we only show the productive pose with the lowest energy.

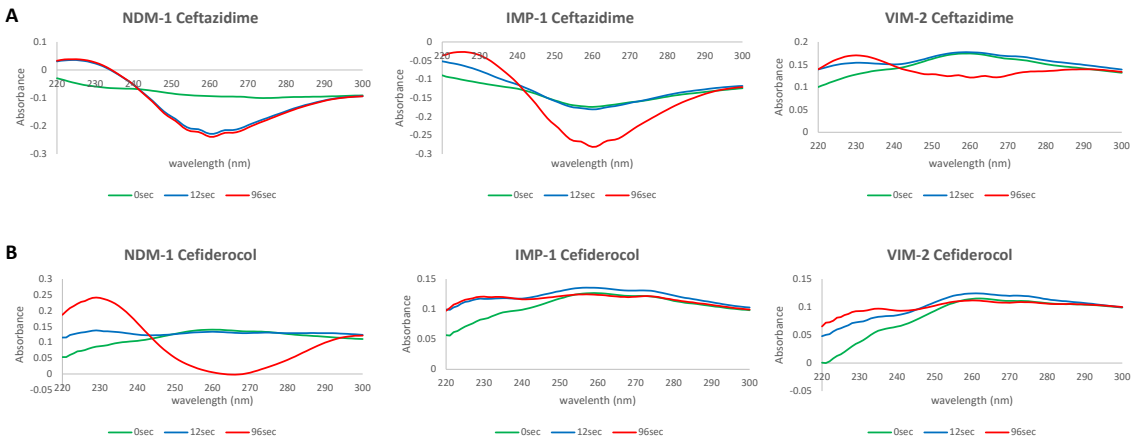

Figure S2. (A) UV difference spectra of ceftazidime with NDM-1, IMP-1, or VIM-2 in a 200:1 *S:E* ratio for 96 seconds. (**B**) UV difference spectra of cefiderocol with NDM-1, IMP-1, or VIM-2 in a 200:1 *S:E* ratio for 96 seconds.

Figure S3. NMR Spectra of FDC and hydrolysis product P1

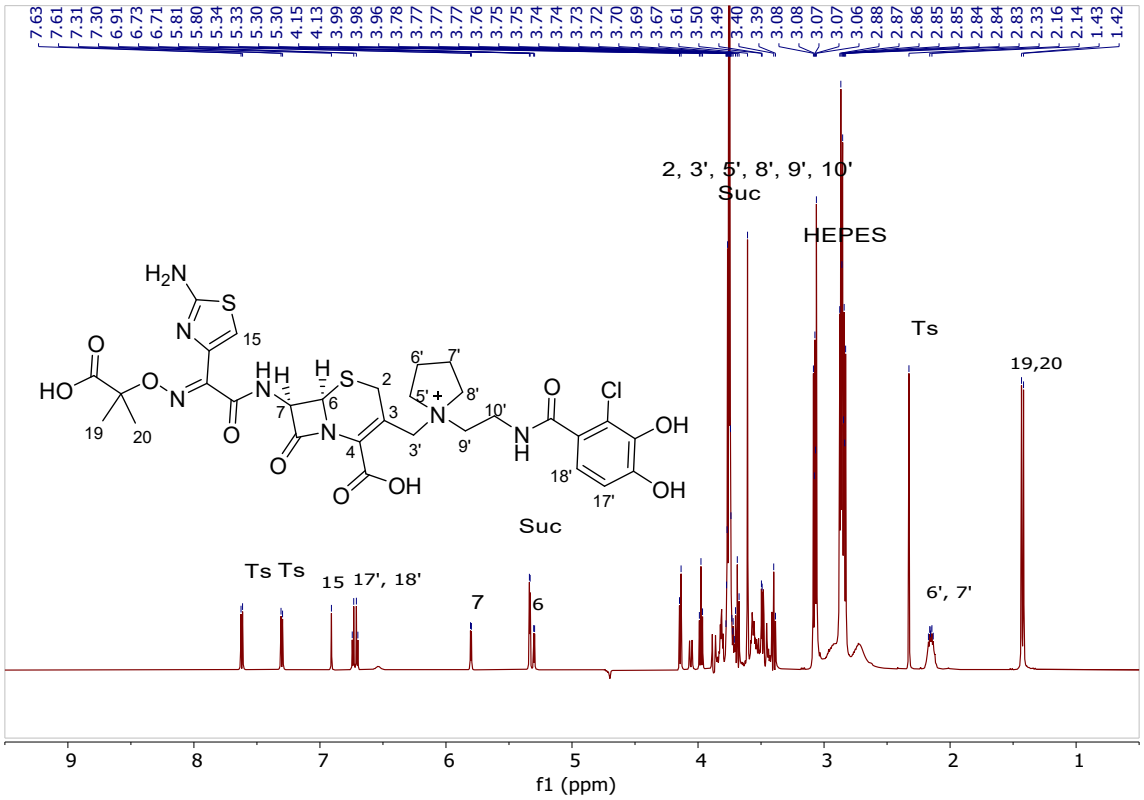

Fig S3A. ^{1}H NMR spectra of FDC containing excipients (sucrose and *p*-toluensulfonic acid) recorded at 700 MHz in HEPES 50 mM pH 7.5 + 10% D_2O.

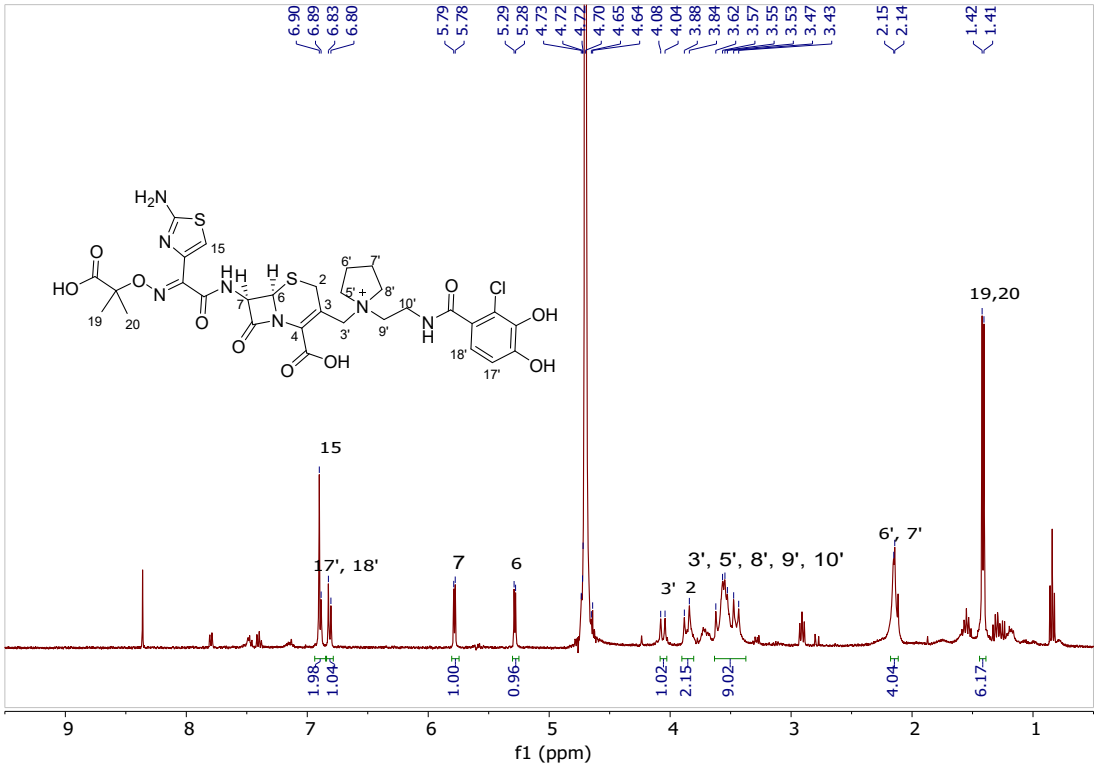

Fig S3B: ^{1}H-RMN of purified FDC in D_2O recorded at 400 MHz.

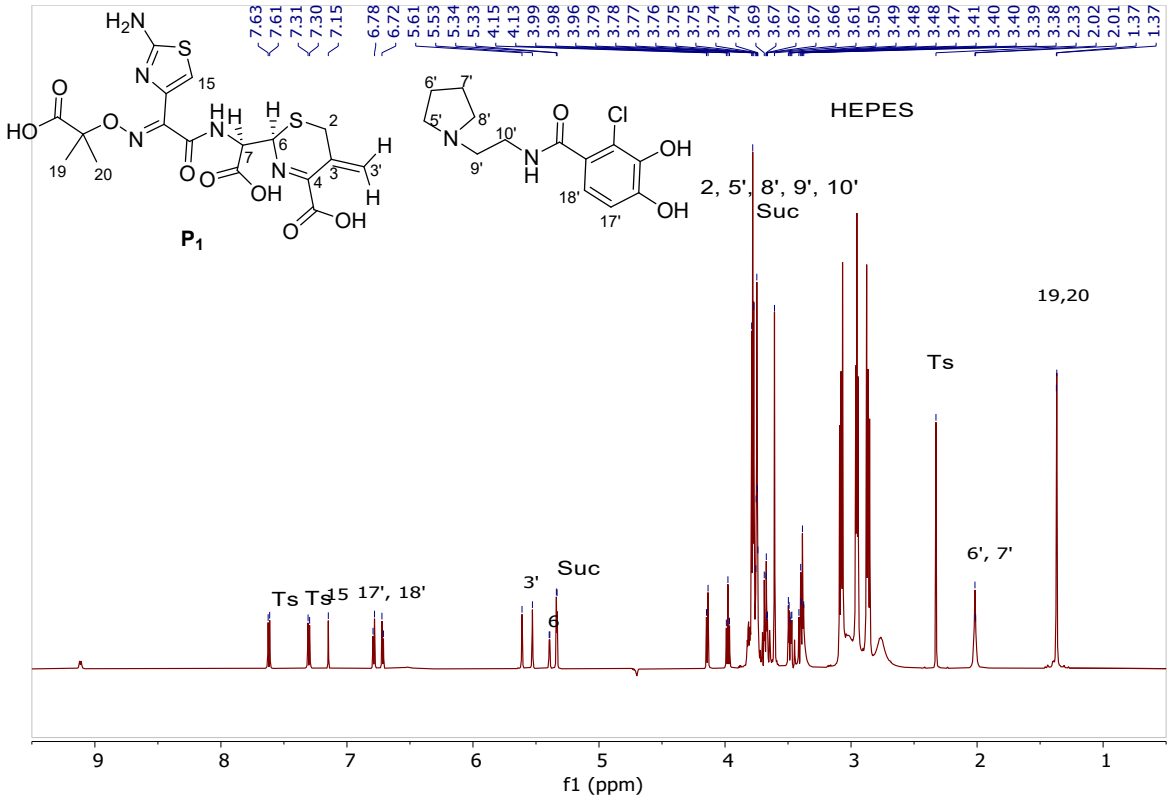

Fig S3C. ^{1}H-RMN of FDC (5 mM) hydrolyzed by NDM-1 (25 µM) with sucrose and *p*-toluensulfonic acid in HEPES 50 mM pH 7.5 + 10% D_2O (700 MHz).

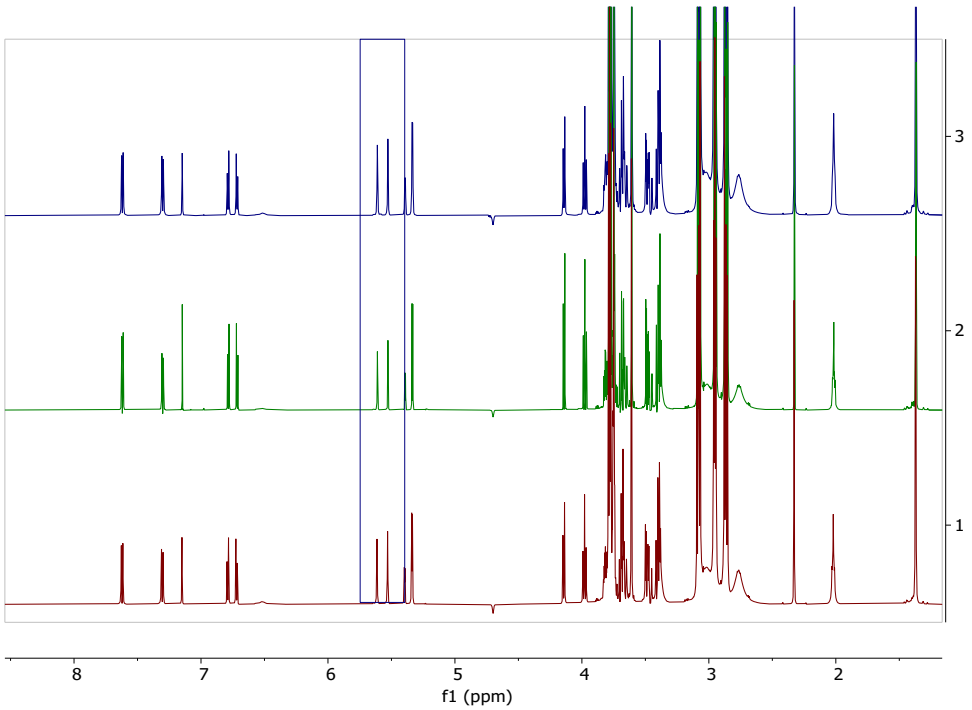

Fig S3D. Comparison of ^{1}H-RMN of enzymatic hydrolysis of FDC (5 mM) by MBL: NDM-1 (20 µM) in blue, VIM-2 (20 µM) in green and IMP-1 (20 µM) in red, showing a common hydrolysis product (P_1).

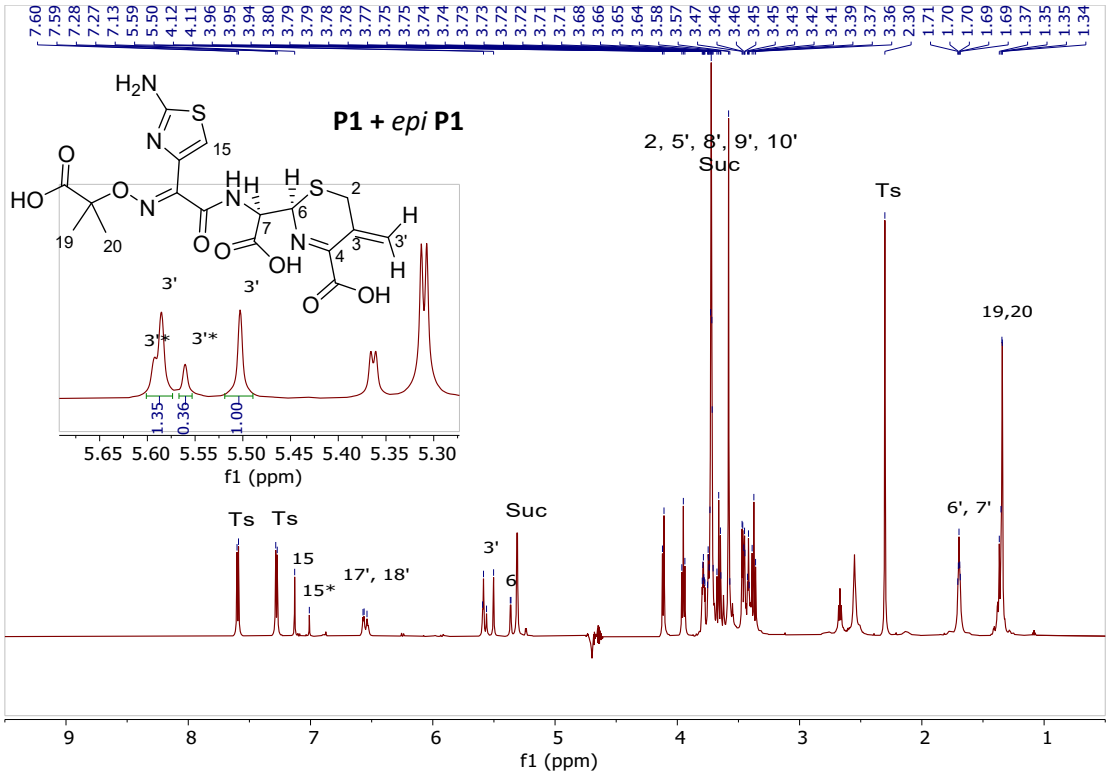

Fig S3E: ^{1}H-RMN of alkaline hydrolysis of FDC (1.2 mM) in its matrix with sucrose and *p*-toluensulfonic acid in NaOH 5 mM pH 11.6 + 10% D_2O (700 MHz). (*) A minor epimer is noted

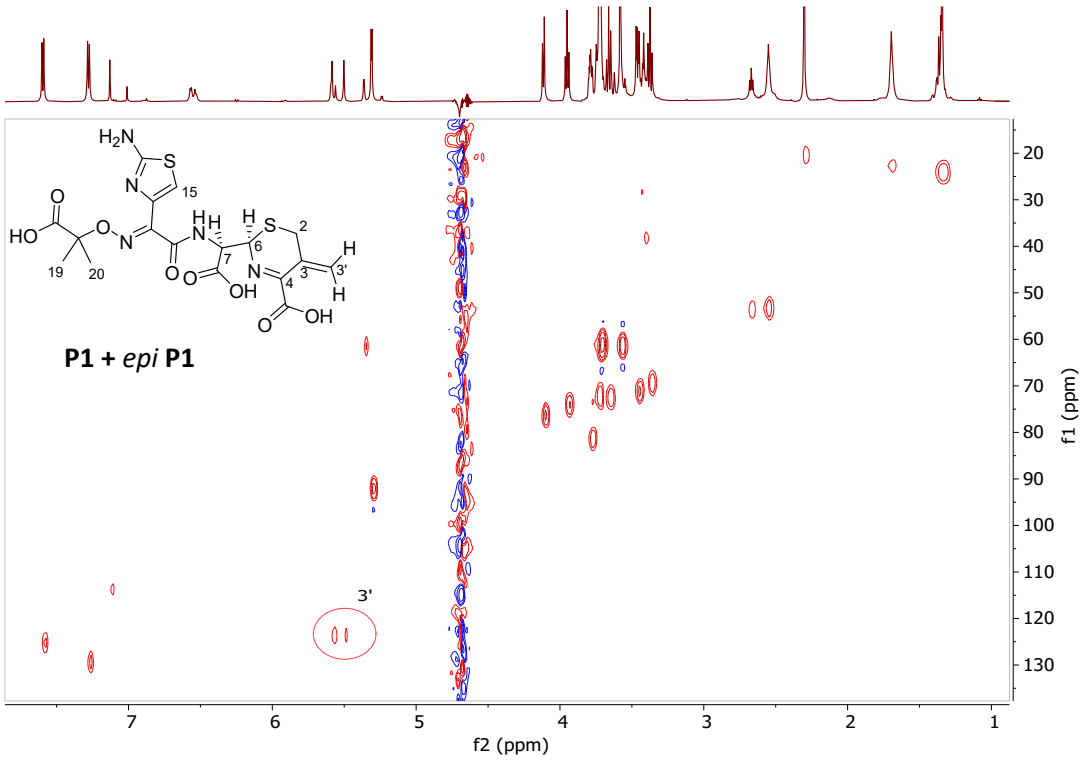

Fig S3F. ^{1}H, ^{13}C, HSQC of hydrolyzed FDC in its matrix with sucrose and *p*-toluensulfonic acid in NaOH 5 mM pH 11.6 + 10% D_2O (700 MHz).

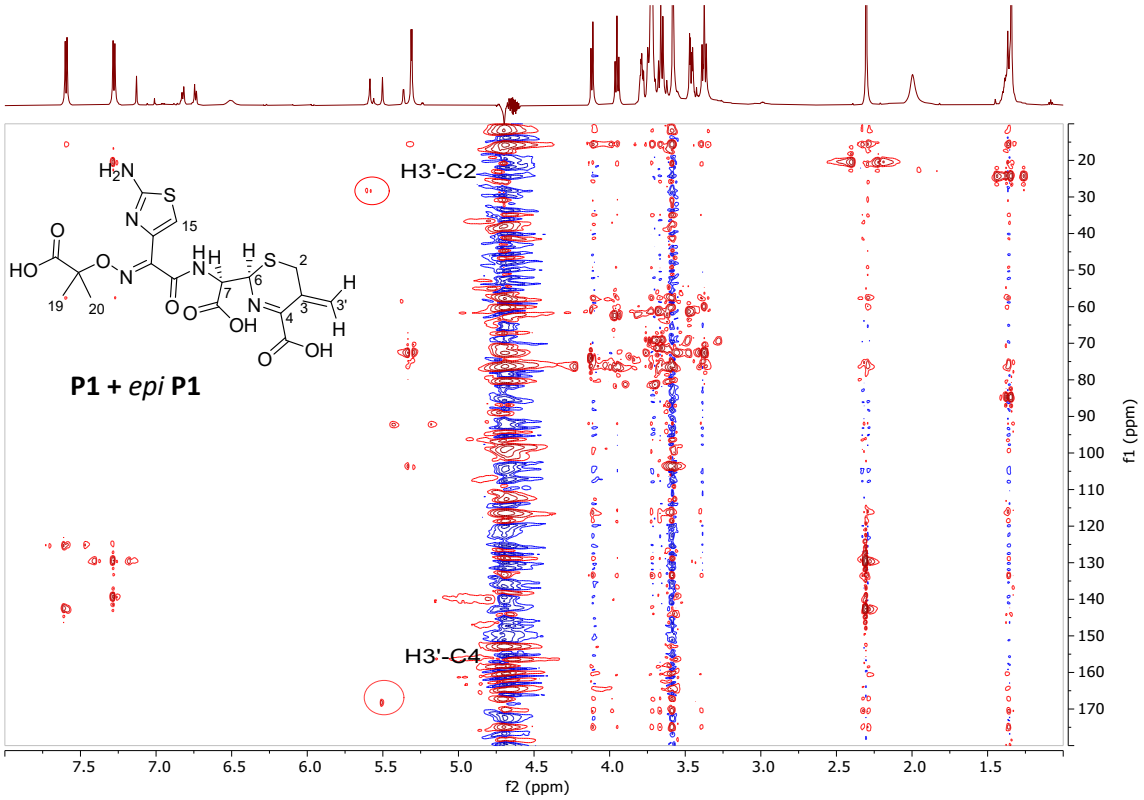

Fig S3G. ^{1}H, ^{13}C, HMBC of hydrolyzed FDC in its matrix with sucrose and *p*-toluensulfonic acid in NaOH 5 mM pH 11.6 + 10% D_2O (700 MHz).

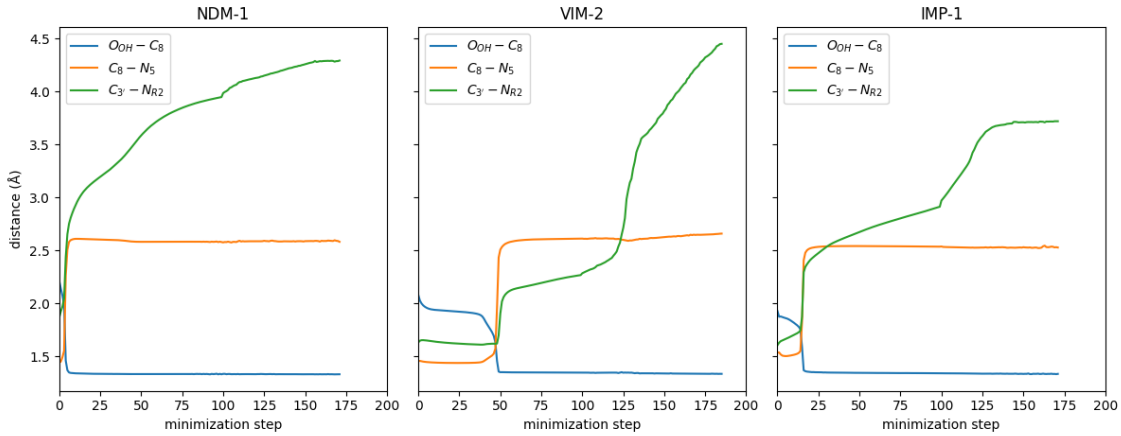

Figure S4. QM/MM simulation of the nucleophilic attack for FDC hydrolysis by NDM-1, VIM-2 and IMP-1. The nucleophilic attack was forced by a harmonic potential to drive the distance between the oxygen atom of the Zn bound hydroxide and the carbon atom of the carbonyl group of the β-lactam ring (shown in blue) to a distance of 1.25 Å. The spontaneous cleavage of the C-N bond in the β-lactam ring is shown in orange, and the lengthening of the C-N bond between the leaving R2 group is shown in green.

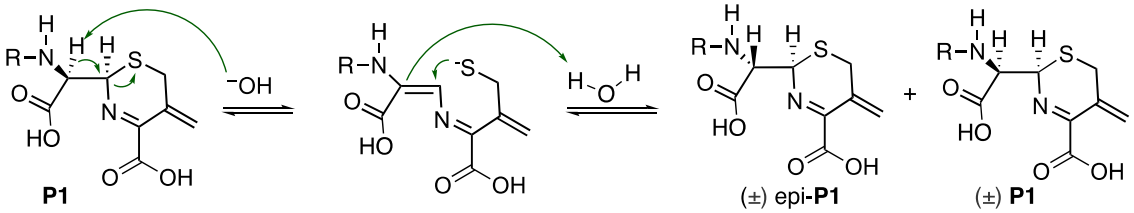

Figure S5. Proposed mechanism for the alkaline-driven P1 epimerization.

Figure S6. NMR Spectra of CAZ and hydrolysis product P1

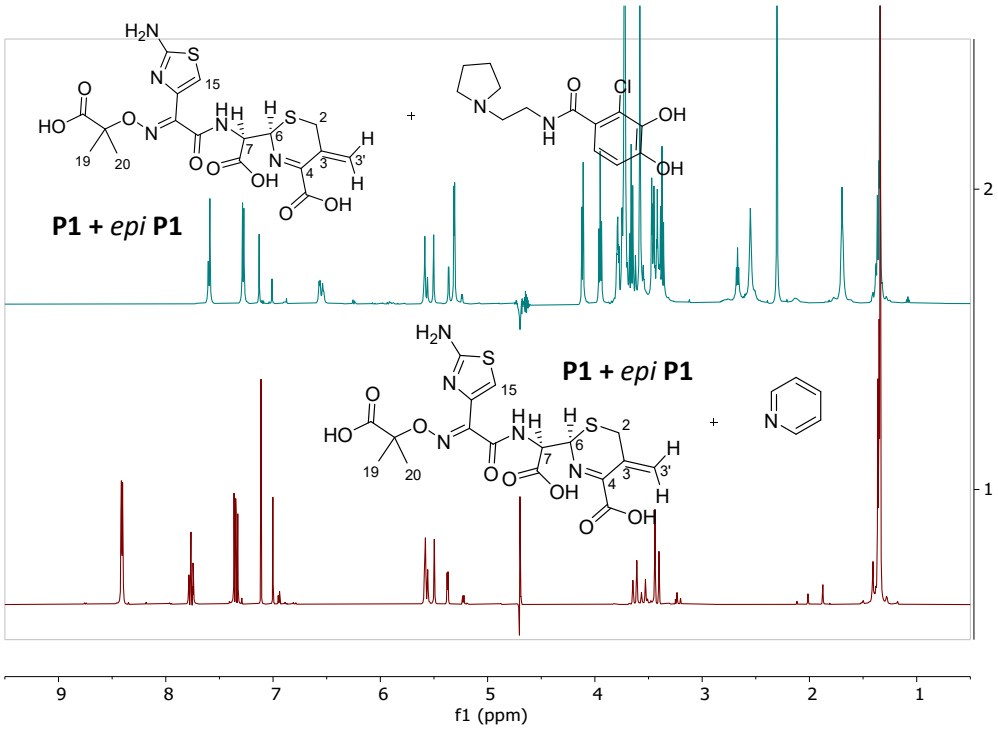

Fig S6A. Comparison of the ^{1}H-RMN spectra of the alkaline hydrolysis product of FDC (1.2 mM in NaOH pH 11.6) in green and CAZ (60 mM in NaOH pH 12) in red, showing a common hydrolysis product.

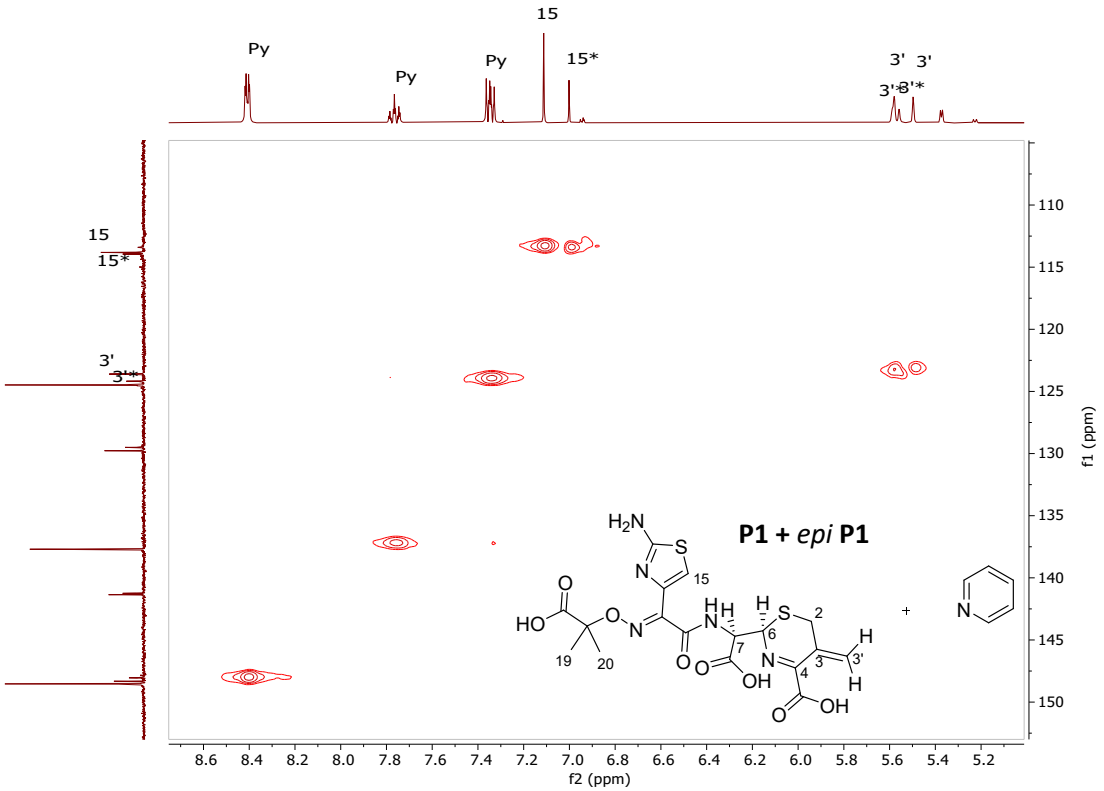

Fig S6B. ^{1}H, ^{13}C HSQC of hydrolyzed CAZ (60 mM) in NaOH 267 mM pH 12 + 10% D_2O (400 MHz). (*) A minor epimer is noted.

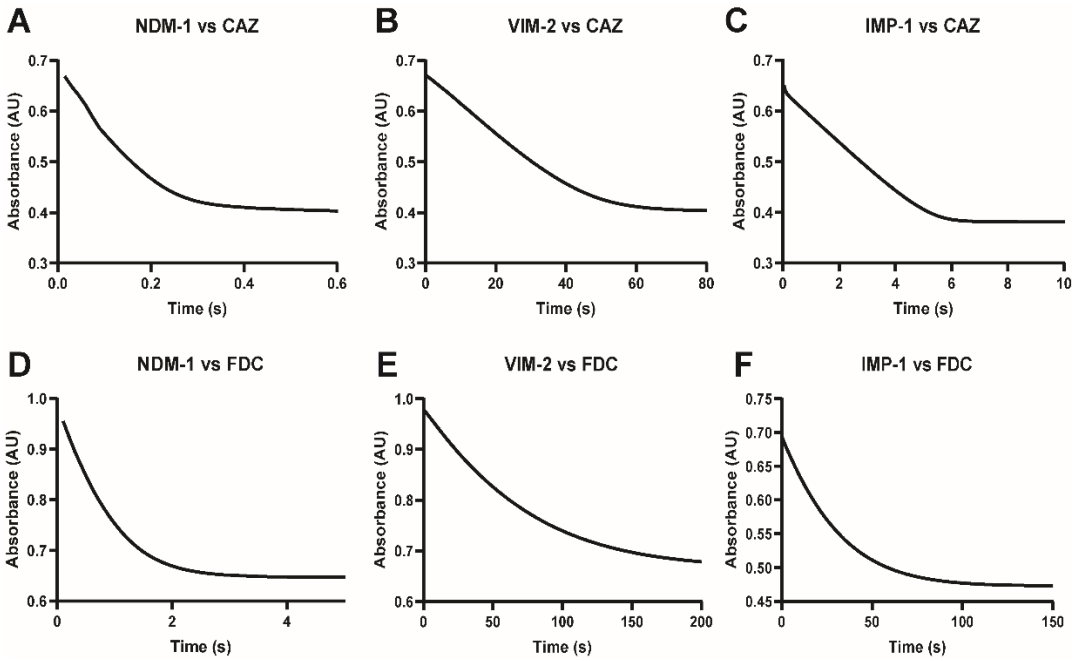

Figure S7. Time frames needed for complete hydrolysis of ceftazidime (A, B and C) and cefiderocol (D, E and F) hydrolysis by NDM-1 (A and D), VIM-2 (B and E) and IMP-1 (C and F). Substrate concentrations were 200 µM and 10 µM of each enzyme in the measurement cell, in buffer HEPES 10 mM, NaCl 200 mM, pH=7.5 supplemented with 20 µM ZnSO4.

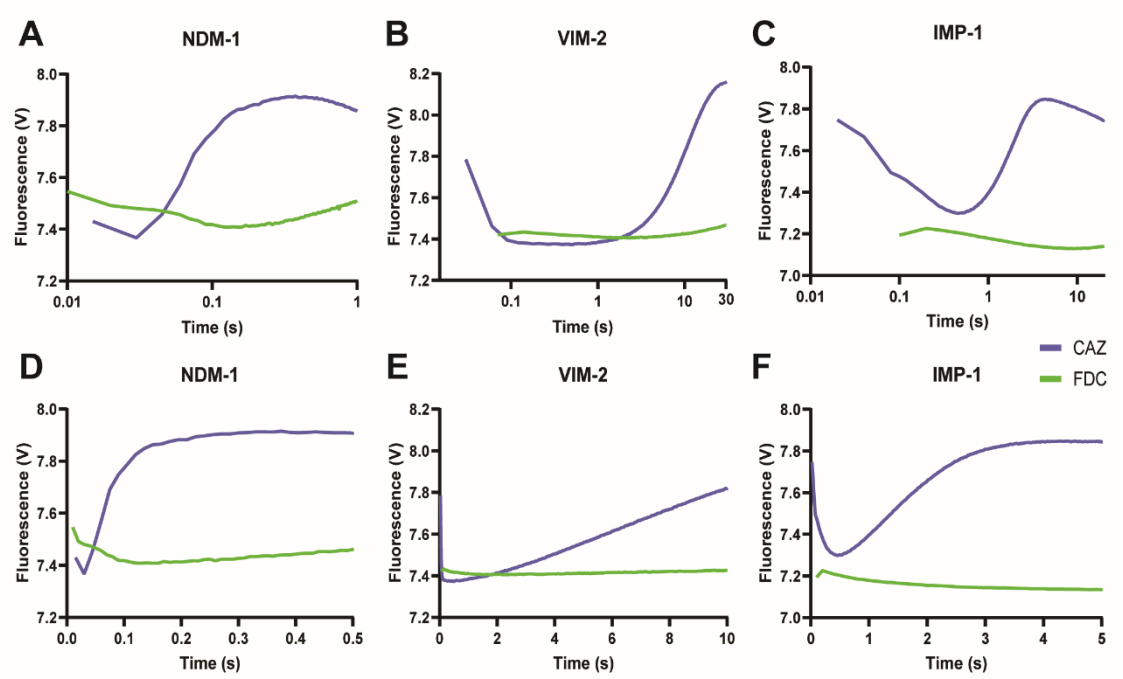

Figure S8. Substrate binding followed by Trp fluorescence. Binding of CAZ or FDC to NDM-1 (**A and D**), VIM-2 (**B and E**) and IMP-1 (**C and F**) were recorded at logarithmic (**A, B and C**) or shorter time scales (**D, E and F**). Binding of CAZ is clearly observable in either scale as fluorescence decays due quenching. Upon complete hydrolysis, intrinsic Trp fluorescence is fully recovered in the free enzyme. In the case of FDC, binding occurs very fast in all cases as initial fluorescence decay occurs in dead time. The slight recovery of Trp fluorescence is first seen for NDM-1 (**A**) at 1 second but this behavior takes 10-fold and 30-fold time for VIM-2 (**B**) and IMP-1 (**C**), respectively.

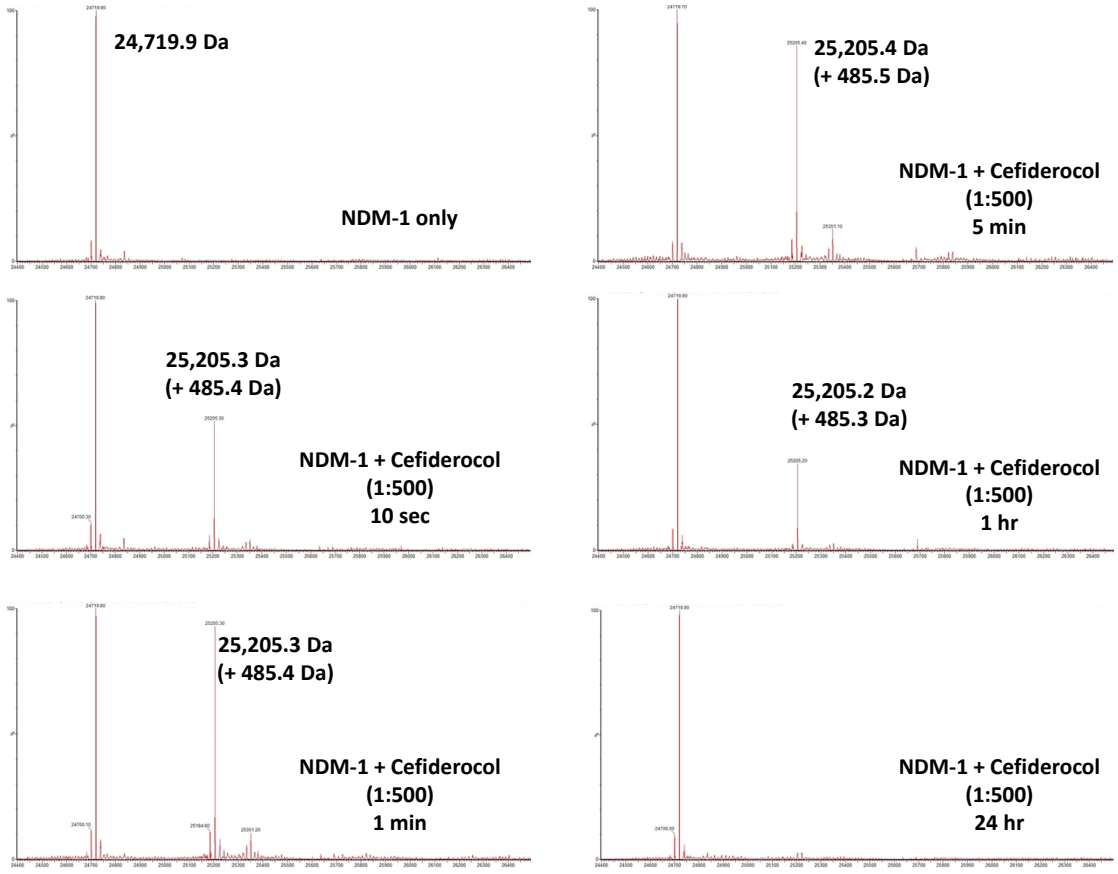

Figure S9. Timed ESI-MS spectra of NDM-1 and cefiderocol (1:500 molar ratio of enzyme-cefiderocol) at timepoints 10 seconds, 1 minute, 5 minutes, 1 hour, and 24 hours.

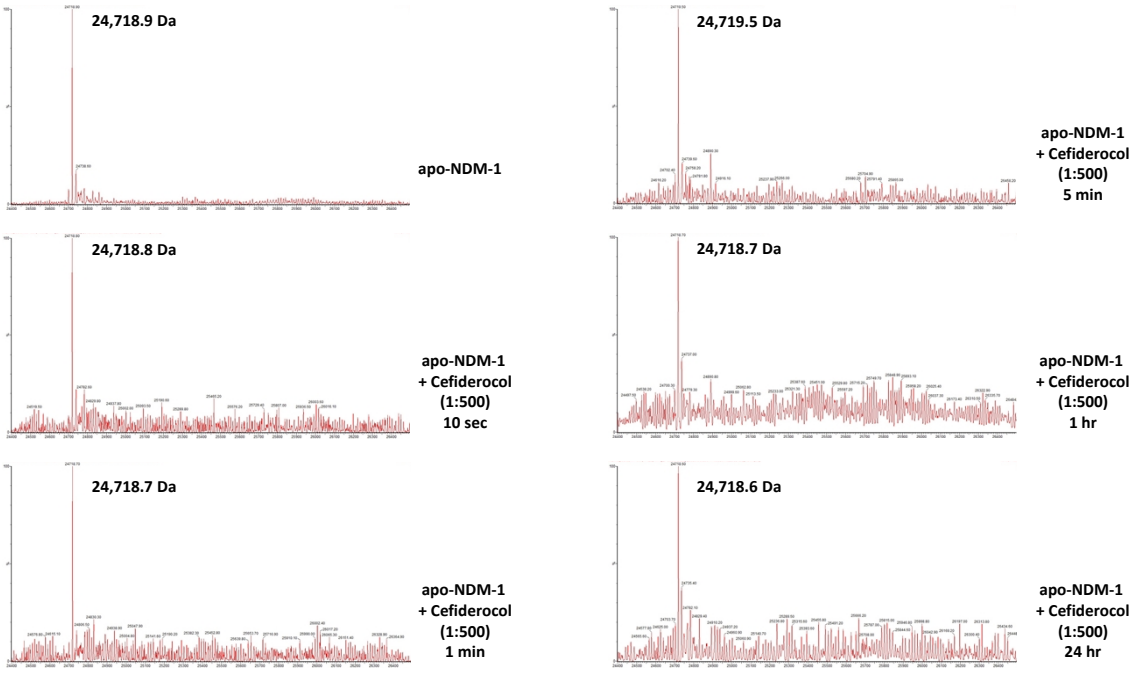

Figure S10. Timed ESI-MS spectra of apo-NDM-1 enzyme with cefiderocol (1:500 molar ratio of enzyme-cefiderocol) at timepoints 10 seconds, 1 minute, 5 minutes, 1 hour, and 24 hours.

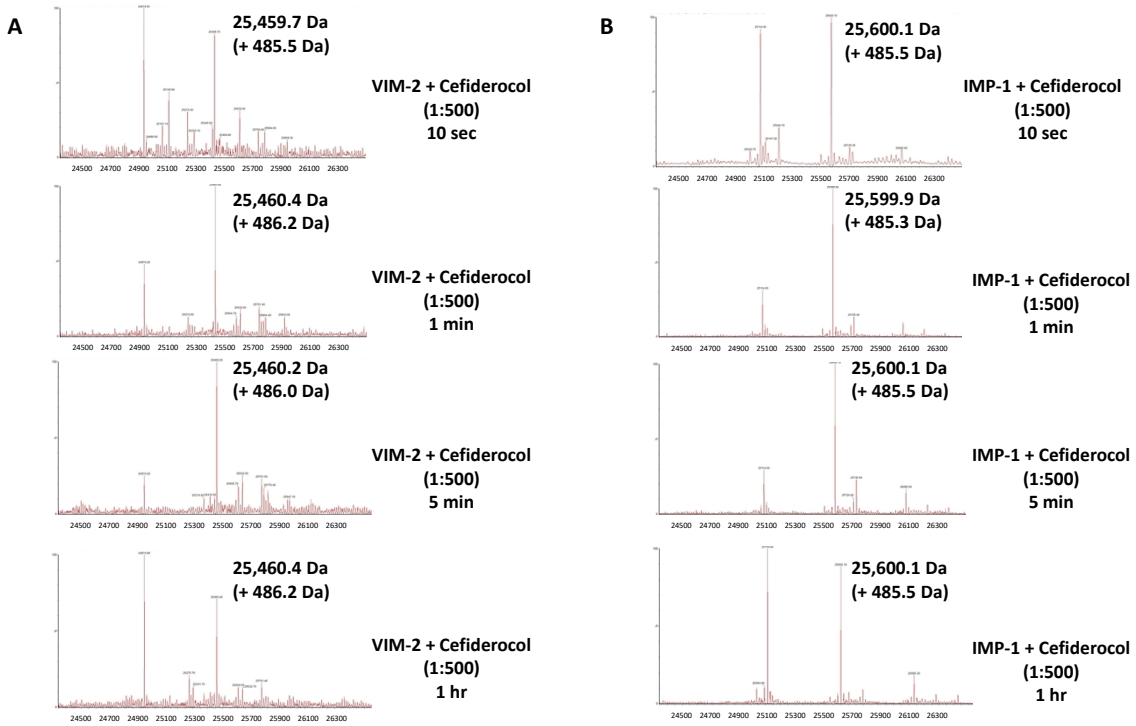

Figure S11. Timed ESI-MS spectra of VIM-2 (**A**) and IMP-1 (**B**) with cefiderocol (1:500 molar ratio of enzyme-cefiderocol) at timepoints 10 seconds, 1 minute, 5 minutes, and 1 hour.

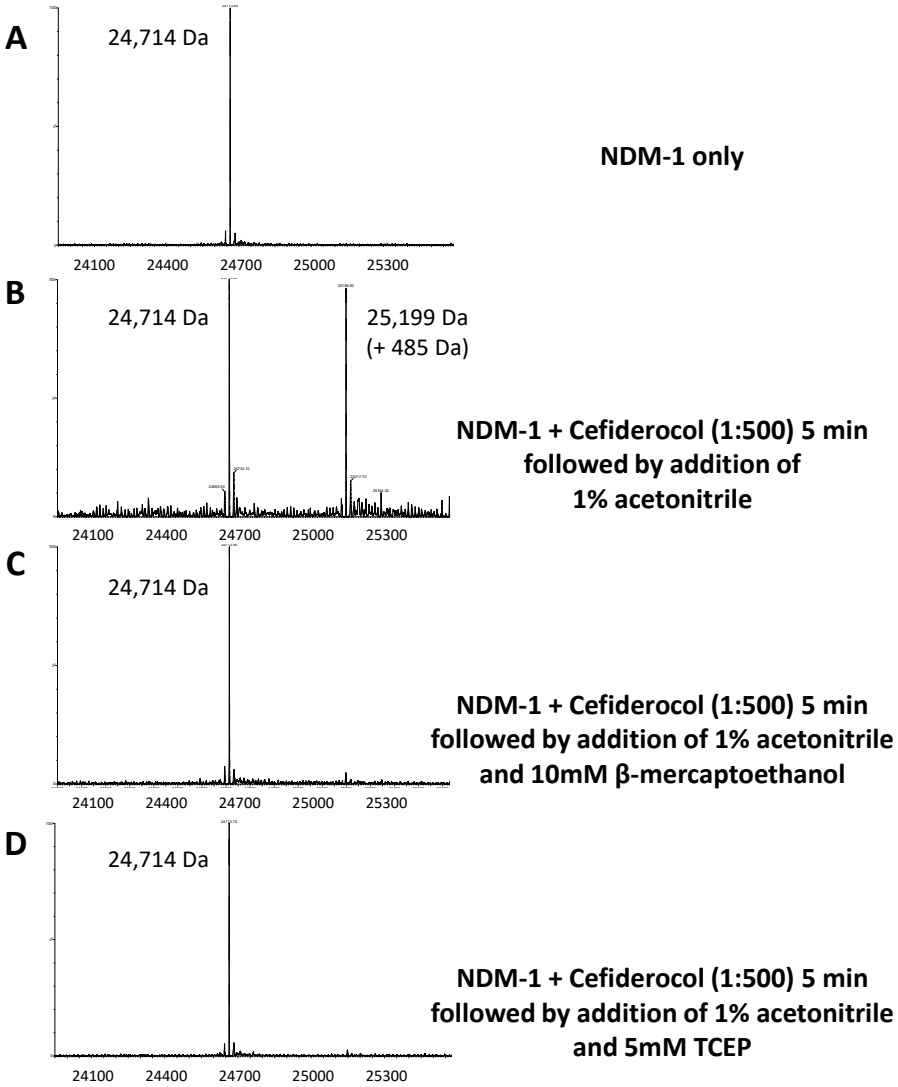

Figure S12. ESI-MS spectra of NDM-1 only (**A**), NDM-1 + cefiderocol (1:500) 5 min followed by addition of 1% acetonitrile (**B**), NDM-1 + cefiderocol (1:500) 5 min followed by addition of 1% acetonitrile and 10 mM β-mercaptoethanol (**C**), NDM-1 + cefiderocol (1:500) 5 min followed by addition of 1% acetonitrile and 5 mM TCEP (**D**). Addition of reducing agents resulted in loss of the +485 Da adduct.

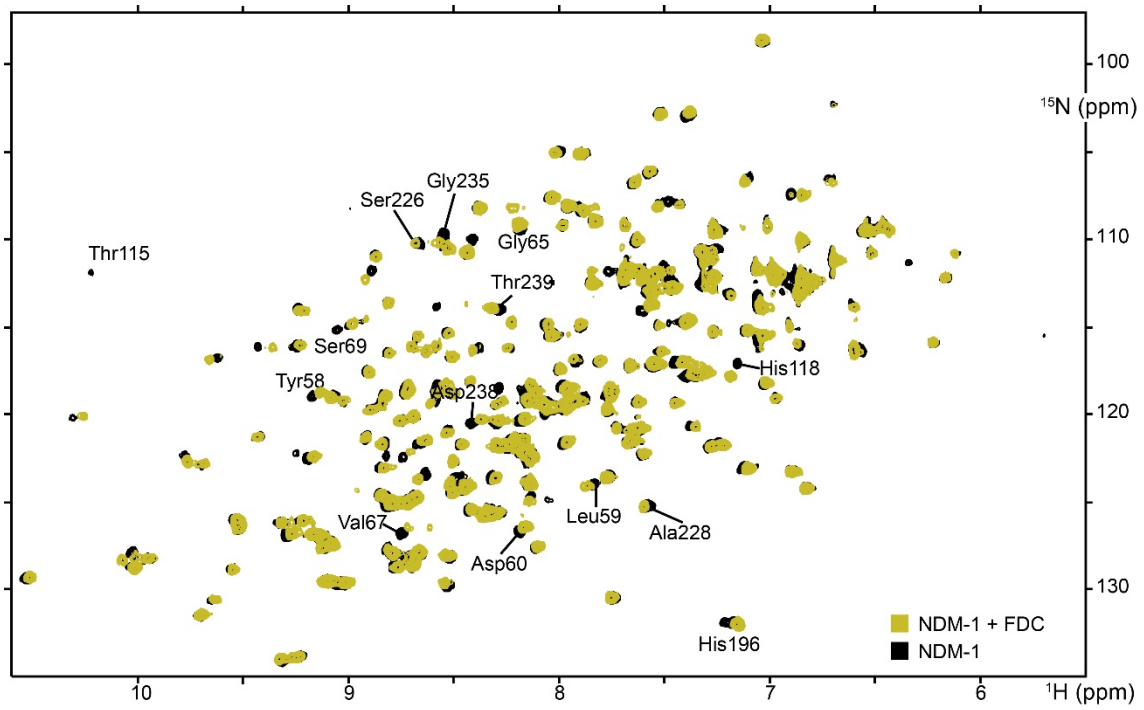

Figure S13. ^{1}H-^{15}N HSQC spectrum of free NDM-1 (300 µM) (black) and bound to FDC (yellow) in a 1:10 ratio. Residues from L3 loop, L10 loop, active site metal ligands or second sphere residues exhibiting chemical shift changes upon FDC addition are marked in the superimposition of spectra in BBL numbering.

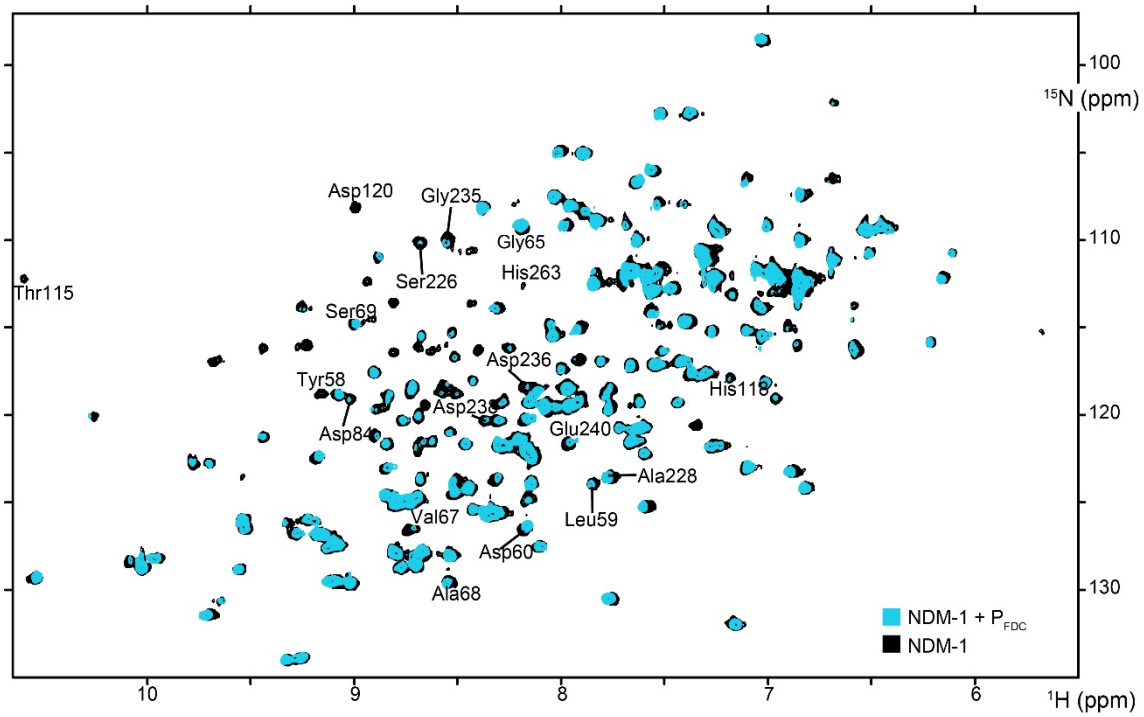

Figure S14. ^{1}H-^{15}N HSQC spectrum of free NDM-1 (300 µM) (black) and bound to P1 (cyan) in a 1:10 ratio. Residues from L3 loop, L10 loop, active site metal ligands or second sphere residues exhibiting chemical shift changes upon addition of P1 are marked in the superimposition of spectra in BBL numbering.

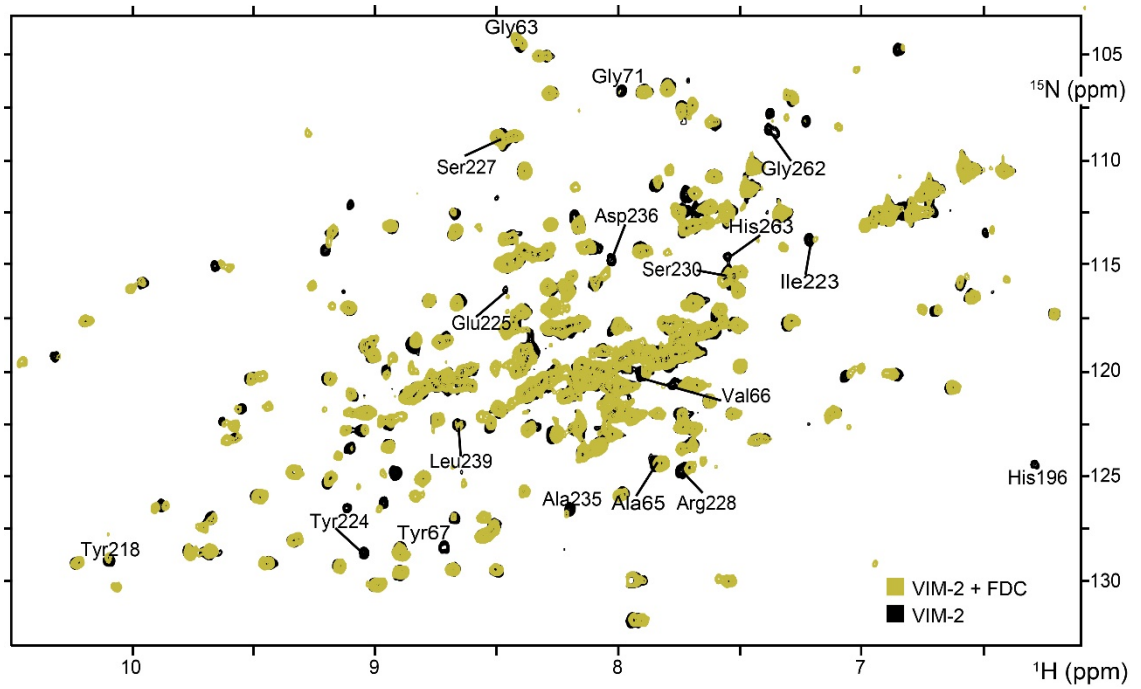

Figure S15. ^{1}H-^{15}N HSQC spectrum of free VIM-2 (300 µM) (black) and bound to FDC (yellow) in a 1:10 ratio. Residues from L3 loop, L10 loop, active site metal ligands or second sphere residues exhibiting chemical shift changes upon FDC addition are marked in the superimposition of spectra in BBL numbering.

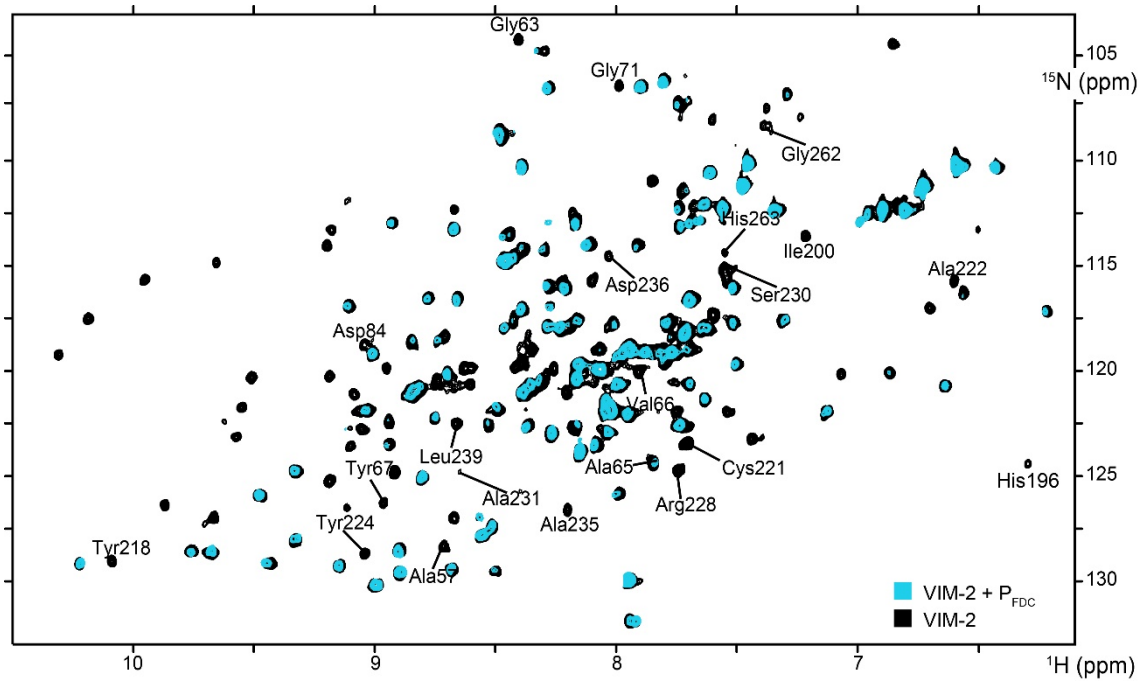

Figure S16. ^{1}H-^{15}N HSQC spectrum of free VIM-2 (300 µM) (black) and bound to P1 (cyan) in a 1:10 ratio. Residues from L3 loop, L10 loop, active site metal ligands or second sphere residues exhibiting chemical shift changes upon addition of P1 are marked in the superimposition of spectra in BBL numbering.

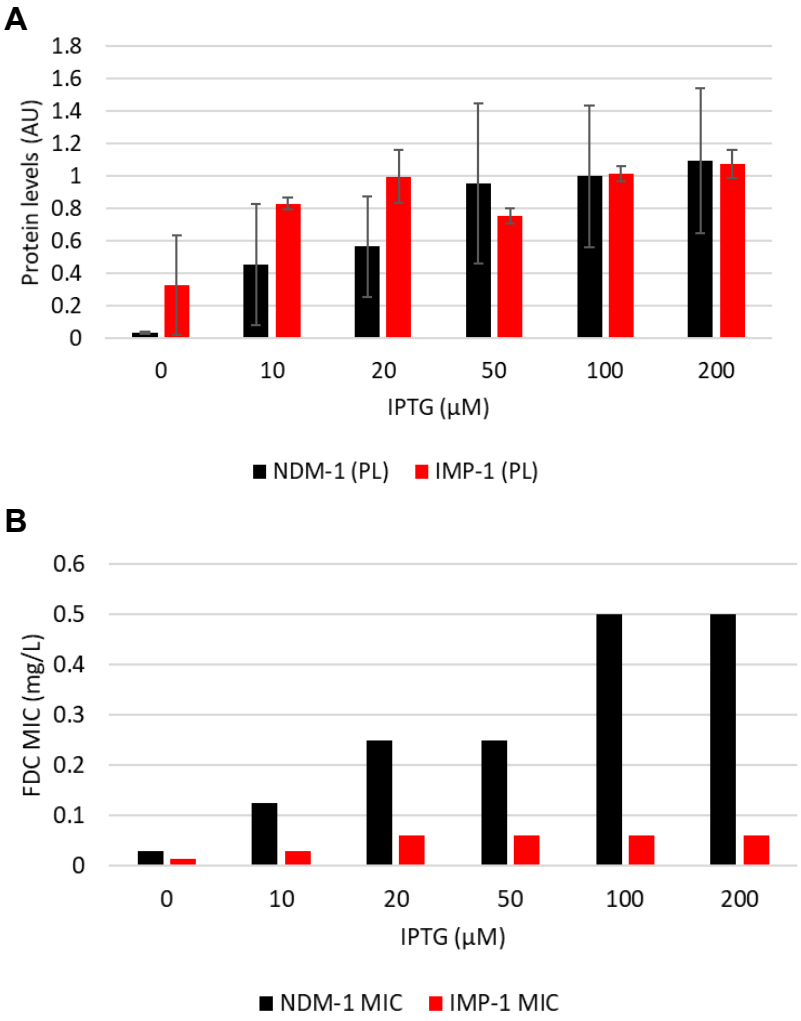

Figure S17. NDM-1 protein levels are associated with increasing FDC MIC values. (**A**) Proteins levels and (**B**) FDC minimal inhibitory concentration (MIC) of *E. coli* DH10B expressing bla_{NDM-1} or bla_{IMP-1} from the IPTG-regulated pMBLe plasmid. Protein levels shown are the mean +/- s.d. of two separate western blots assays prepared from the MIC assays. MIC values are the mode of at least three biological replicates.

References

1 A. Birgy, C. Nnabuife and T. Palzkill, *Antimicrob. Agents Chemother.*, 2024, **68**, 1–13.

2 M. Ruggiero, I. Briceño Muñoz, G. Gutkind, A. M. Hujer, R. A. Bonomo and P. Power, *Antimicrob. Agents Chemother.*, 2024, **68**, e0172023.

3 A. Kawai, W. C. Shropshire, M. Suzuki, J. Borjan, S. L. Aitken, W. C. Bachman, C. L. McElheny, M. M. Bhatti, R. K. Shields, S. A. Shelburne and Y. Doi, *MBio*, 2024, **15**, e0287423.

4 S. Gaillot, S. Oueslati, J. B. Vuillemenot, M. Bour, B. I. Iorga, P. Triponney, P. Plésiat, R. A. Bonnin, T. Naas, K. Jeannot and A. Potron, *Front. Microbiol.*, 2023, **14**, 1253160.

5 C. Lasarte-Monterrubio, P. Guijarro-Sánchez, J. C. Vázquez-Ucha, I. Alonso-Garcia, L. Alvarez-Fraga, M. Outeda, M. Martinez-Guitian, A. Peña-Escolano, R. Maceiras, E. Lence, C. González-Bello, J. Arca-Suárez, G. Bou, A. Beceiro, I. Merino, E. Cercenado, R. Gómez, T. Soler, I. Gracia-Ahufinger, L. Martín, F. Galán, N. Tormo, J. C. Rodríguez, S. Capilla, F. Marco, M. D. Quesada, E. Padilla, F. Tubau, J. González, A. I. López-Calleja, J. L. del Pozo, M. I. García, M. Martinez, J. Calvo, X. Mulet, F. Peña, A. I. Rodríguez, M. J. Gude, A. Fernández, J. Fernández, F. Fernandez-Cuenca and A. Pascual, *Antimicrob. Agents Chemother.*, 2023, **67**, e0150522.

6 X. Liu, T. Lei, Y. Yang, L. Zhang, H. Liu, S. Leptihn, Y. Yu and X. Hua, *Antimicrob. Agents Chemother.*, 2022, **66**, 1–6.

7 T. Ito-Horiyama, Y. Ishii, A. Ito, T. Sato, R. Nakamura, N. Fukuhara, M. Tsuji, Y. Yamano, K. Yamaguchi and K. Tateda, *Antimicrob. Agents Chemother.*, 2016, **60**, 4384–4386.

8 A. Kawai, C. L. McElheny, A. Iovleva, E. G. Kline, N. Sluis-Cremer, R. K. Shields and Y. Doi, *Antimicrob. Agents Chemother.*, 2020, **64**, e00198-20.